



Development of a Mathematical Model Using Machine Learning for Hydroforming of Non-Circular Protrusion Copper T-Tube

Moataz El-Shazly^{1,*}, Mostafa Shazly², Tarek Osman³

¹Mechanical Design and Production Department, Faculty of Engineering, Cairo University, Giza 12613, Egypt

²Mechanical Engineering Department, Faculty of Engineering, The British University in Egypt, Al-Shorouk City, Cairo 11873, Egypt

³Mechanical Design and Production Department, Faculty of Engineering, Cairo University, Giza 12613, Egypt

ARTICLE INFO

Article history:

Received:13-11-2020

Accepted:26-11-2020

Online:30-11-2020

Keywords:

Tube hydroforming

Machine learning

Multiple ridge regression

Loading path

Wrinkling

ABSTRACT

Optimum loading paths for successful tube hydroforming processes have been studied by several researchers. In this paper, an adaptive, heuristic, nonlinear mathematical model (AHNM) was proposed to optimize the loading path of a hydroforming process through adaptive minimization of the internal pressure and axial load of the process. Firstly, Finite Element Analysis (FEA) was used to analyze the hydroforming process where several features of the process were extracted from the FEA for further analyses of the relations among them. To capture these relations and include them in the AHNM, the paper examined several Machine Learning algorithms including Multiple Linear Regression, Multiple Ridge Regression, Decision Tree, and Random Forest. The Multiple Ridge Regression was found to give the highest accuracy to efficiently linear modelling the inputs and outputs of the FEA of the hydroforming process. The AHNM model was implemented, solved, and optimized using several steps of tee protrusion height that create several loading paths. It was found that increasing the number of steps and starting with small increment leads to minimizing the system requirements.

1. Introduction (Heading 1)

Tube Hydroforming (THF) is a special type of die forming that was invented by Gray, Devereaux, and Parker [1] to manufacture seamless copper fittings with T-protrusions using a combination of internal pressure and axial load to produce defect-free parts. These defects were either failure by rupture (bursting) due to excessive internal pressure or wrinkling due to excessive axial loads.

To avoid process failure, several studies analytically investigated the loading path. These analytical solutions are useful for simple geometries only. Besides, many trial-and-error simulations may be required to obtain acceptable loading paths, which is both time and cost-inefficient. Literature review of the state-of-the-art which investigated the relations between process variables could be found in [2-4], also Reddy [5] studied the

effect of tube material and heat treatment temperatures on tube hydroforming process.

Guidelines for employing finite element modelling (FEM) in the process simulation were presented to predict the effect of process parameters. Other studies focused on determining the criteria to avoid major failure modes. Furthermore, several control techniques such as fuzzy logic had been implemented with the several algorithms such as Genetic algorithm, Simulated Annealing, Response Surface Method, Steepest Descent, Pareto, Line-Search and Bisection Methods, artificial neural network modelling...etc., utilized finite element simulations to predict the input parameters that would produce the desired hydro formed tube [6-11]

Continuous development resulted in hydroforming modelling process based on adaptive process simulation. These processes use an incremental procedure to detect the onset of defects, where at the end of each increment, load values are modified for the

*Moataz El-Shazly, Faisal, Giza, 01271915198, moatazmech@gmail.com

subsequent increments. Process parameters are adjusted to avoid the onset of wrinkling and bursting using Controlled Algorithms [12-16], Genetic algorithm (GA) by Abedrabboa et al. [17].

To conclude, wrinkle formation during the hydroforming process was mainly detected using two approaches: the instability theory or real-time sensing. Unfortunately, these methods cannot be generalized and could be only used during the free-forming phase. Besides, they cannot differentiate between wrinkles and die features with crooked details. Therefore, a more robust wrinkling criterion for T-tube hydroforming should be used to mathematically determine the amount of wrinkling while optimizing the hydroforming loading path. Furthermore, elliptical protrusions (used in this paper) received little attention in the literature despite its importance in the manufacturing of some industrial applications such as Tee-joints for automobiles and bicycles chassis. Moreover, the implementation of such forming hydroforming process necessitates the use of physical sensors along with an active control system and optimization tool to analyze and predict the wrinkling and thinning, and hence act accordingly. This adapted process is expensive in software, data acquisition system, and physical sensors, which are considered shortcomings.

The objective of the present work is to tackle these expensive complex systems by predicting the optimum loading path for a T-tube hydroforming process of a circular tube with an elliptical protrusion. This is achieved by proposing an approach to combine finite element simulations and Machine Learning Techniques to express the relations between the process parameters, and then apply an adaptive heuristic nonlinear mathematical model (AHNM) that takes into consideration the problem objective function to minimize the pressure and the applied axial load. The problem constraints are the wrinkling and the thinning measures.

2. Adaptive Heuristic Framework

The hydroforming process is modelled in the adaptive heuristic nonlinear mathematical model (AHNM) by using machine learning algorithms (MLA). MLA will learn the causal relations between different parameters to formulate mathematical forms and then optimize them. Taking into consideration the wrinkling and thinning indicators, the adaptive heuristic framework proposed in this paper, Figure 1, solves the need for real-time data or depends on historical data by using machine learning algorithms (to be discussed in Section 2.3) to map the relations between inputs and outputs of the FEA of the hydroforming process. Doing that, a machine learning algorithm trained on an FEA dataset would be able to predict the behavior of the material under hydroforming, thus removing the need for historic or real-time data. There are two possible routes for the hydroforming optimization model. If the output of the machine-learning algorithms cannot be explicitly formulated in equations or inequalities, i.e., machine learning algorithms are represented using specific data structures that cannot be simplified into explicit equation or inequalities; the best solution is to combine an iterative optimization algorithm as discussed in the literature (e.g. Genetic algorithm). On the other side, if the machine learning algorithms could be explicitly formulated, the preferred

route is the Adaptive heuristic nonlinear mathematical (AHNM) model, where the equations obtained from the ML could be integrated into a closed-form, mathematical optimization model as constraints.

As usual for most mechanical engineering and research problems, approximation could be used to either simplify calculations of complex relationships or to help build new models or both. In this research, linearity was assumed, linearity facilitated the incorporation of the finite element model represented by the trained machine learning model into the AHNM model.

Similar research in the literature avoided reporting the time of the finite element analysis when being used to obtain optimal loading path, due to these times being extensively long. In this research, by representing the finite element behavior of the hydro formed tube using machine learning model. Any new analysis of the hydro formed tube for new pressures and axial loads became “instants” with separable variables that could be integrated into a mathematical model. This is unprecedented and extremely helpful when formulating mathematical models similar to what is presented in this research.

2.1. FEA model

The case study investigated here is a hydroforming process of a tube where a straight tube is hydroformed to T-joint with an elliptical protrusion. The FEA of the hydroforming process is performed using Simulia® 2020. A seamless copper tube ASTM B88, CU-C12200 (Alloy C12200 Cu=99.90% minimum, P=0.015- 0.040%) produced by SAMPOTUBE is used. The tube used has an outer diameter of 22.22 mm, an initial length of 110 mm, and a tube wall thickness of 0.2 mm. The elliptical T-branch major and minor diameters are 40 and 22.22 mm, respectively. The mechanical properties of the material are shown in Table 1. Figure 2 shows the dimensions of the final product and due to the symmetry of the model, only a quarter model is used as shown in Figure 3 to decrease the FEA solution time.

The mould consists of two parts, a holder which rests on the protrusion zone to prevent its bursting, and a mould cavity where the tube will be formed. These two parts are modelled as 3D discrete rigid parts while the tube blank is treated as 3D deformable thin shell, Abdelkefi [18]. The contact between the tube and the die surfaces is assumed to be frictionless contact with boundary conditions as shown in Figure 3.

The die is completely fixed, and the holder can move vertically in Y-direction only. Edge A is constrained to move in the Z-direction, while Edge B is constrained to move in the Y-direction only, and Edges C can move in ZY-plane. Figure 3(b) shows the applied axial load (N/mm) on Edge A, and Figure 3(c) shows the applied internal pressure (MPa) on the internal surface of the tube. A mesh sensitivity analysis is conducted and summarized in Table 2 which shows that a model with an element size of 0.8 mm is appropriate for both thickness accuracy and solution time.



Figure 1: The Adaptive Heuristic Framework Proposed

Table 1: Copper Tube Material Properties

Density	8940 Kg/m ³
Yield strength (Sy), Tensile strength (Su)	276.0, 310.0 MPa
Modulus of elasticity (E)	117 GPa
Poisson ratio	0.33
Strength Coefficient (K)	315.0 MPa
Strain hardening exponent (n)	0.54

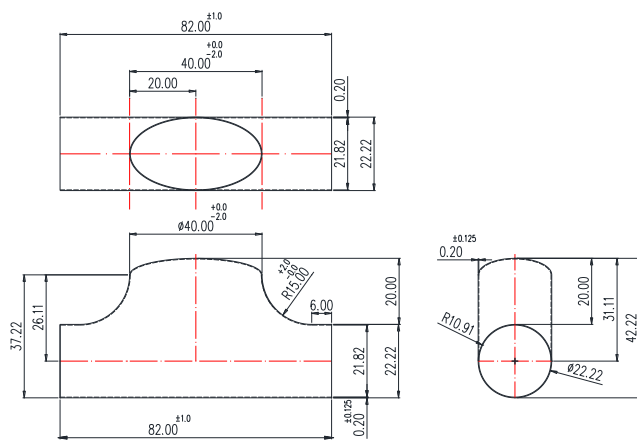


Figure 2: Dimensions of the final product

Based on the iterative process proposed in Figure 4, the values of both the internal pressure and axial load are obtained to produce a wrinkle-free hydro formed tube with the elliptical protrusion. Figure 5 demonstrates a successful implementation of the model developed in Figure 4, where no wrinkling happened at the end of the process. The minimum thickness of the hydro formed tube is 0.155 mm, and the protrusion height is 21.5 mm.

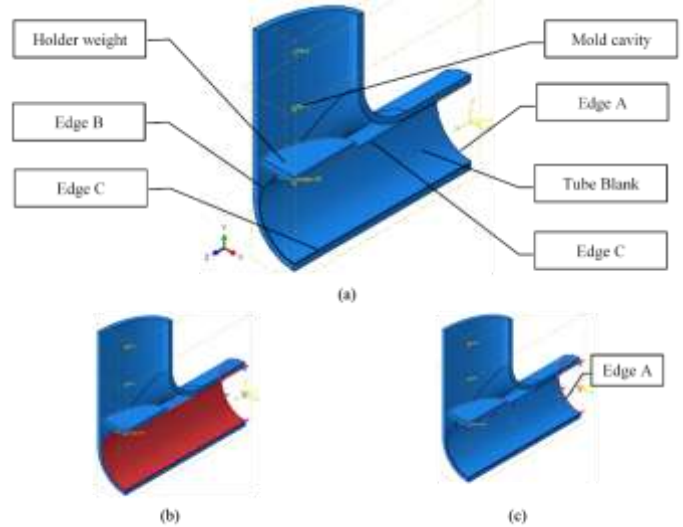


Figure 3: FEA Model (a) Boundary Conditions Applied to The Model, (b) Applied Internal Pressure On the Tube Surface, (c) Applied Axial Load on Tube Edge

Table 2: Results of Mesh Sensitivity Analysis

Mesh size, mm	Solving time, min.	Min. Shell Thickness, mm	Difference, mm
2.00	2	0.1612	
1.50	3	0.1587	0.0025
1.00	8	0.1572	0.0015
0.80	13	0.1559	0.0013
0.60	27	0.1551	0.0008
0.50	44	0.1549	0.0002

Machine learning algorithms require sizeable data amount that depends on the problem being solved. For the present case study, it is suggested to obtain the data of 75 cases to train the machine learning algorithms. A Python script was developed to interact with ABAQUS, to iteratively change the internal pressures and the axial loads, perform the FEA, and extract the results. The range of the internal pressures and axial loads were selected based on the successful initial FEA model to be from 3 to 7 MPa for the internal pressure, and 26 to 40 N/mm for the axial load (Appendix-A). The FEA outputs included the minimum and maximum wall thickness of the tube, the maximum vertical displacement of the protruded section; average kinetic energy, average internal energy, maximum and the second principal stresses, and the maximum strain in the deformed non-

circular part. A total of 57 simulations were performed successfully.

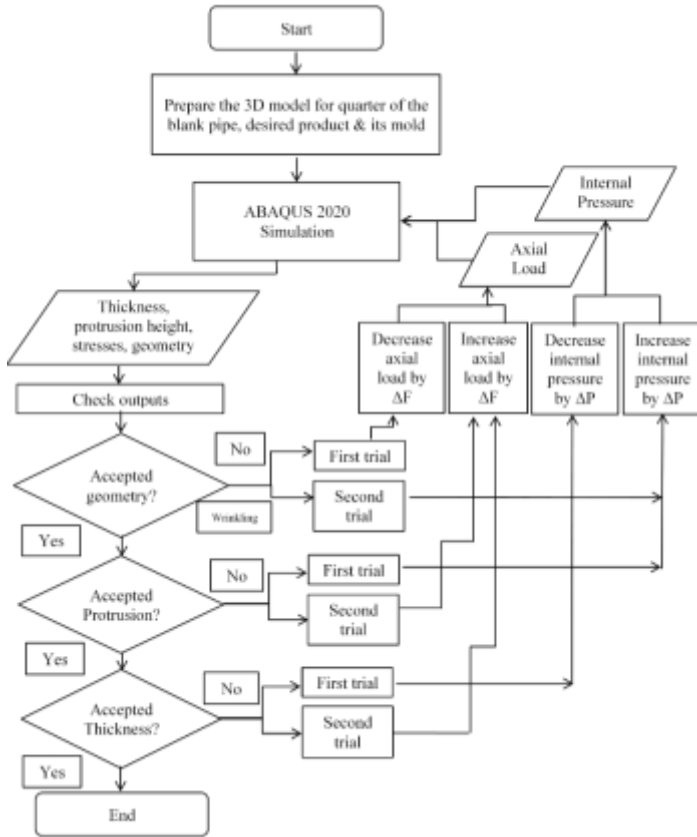


Figure 4: Flow Chart of the Iterative Process Proposed to Produce the Initial FEM

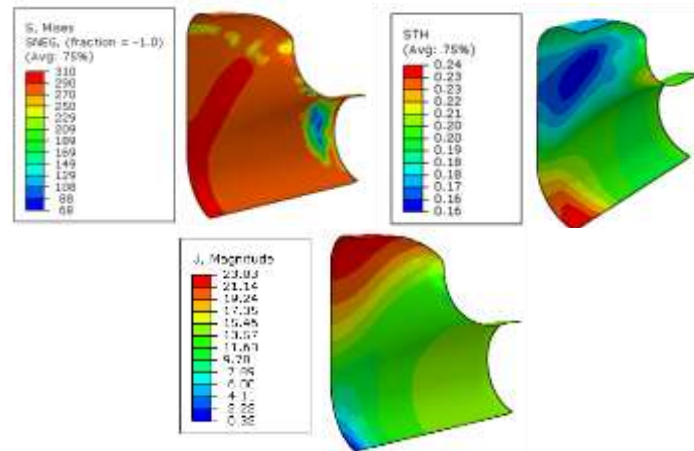


Figure 5: Stress distribution, Displacement distribution, and Thickness distribution of the simulated model

2.2. Machine learning algorithms

This paper focuses on supervised learning (the input and the outputs of the process are known and labelled) as detailed in subsections. ML is not by itself an optimization tool. The main purpose of ML in this paper is to describe the FEA dataset

obtained and then predict the FEA output that would not violate the hydroforming optimization model proposed in Section 2.3.

In the literature, the use of the open-source machine learning library Scikit-Learn in the mechanics' field allows to examine different algorithms and obtain the best one, A. Bessa [19]. The algorithms that could be implemented using Scikit-Learn require 50 data samples at least ("As of July 2020, scikit-learn.org, scikit-learn algorithms") [20] (in this paper, 57simulations are used) to train the algorithms.

Several algorithms are available including regression models, decision tree and random forest. Regression analysis is a statistical technique that models and approximates the relationship between a dependent and one or more independent variables. Regression models used include linear regression, ridge regression, lasso regression, and elastic net regression are discussed by Andreis [21]. Linear regression attempts to minimize the sum of the error squared between the predicted and actual data. Decision Tree and Random Forest are two known and robust machine learning algorithms that have different regression algorithms, Prajwala [22]. Both algorithms could be also used to infer relations between features in a dataset. Random forest is considered a collection of decision trees, where each tree describes a subset of the data provided to the random forest algorithm. Normally, the dataset features represent different characteristics (inputs and outputs) of a specific case study.

2.3. Machine learning algorithms results

The variable constituting the inputs and the outputs of the machine learning algorithms are also used in the AHNM model discussed. It is also noteworthy that these variables are those extracted from the FEA 57 runs. Normally, the machine learning algorithms discussed above could only deal with several inputs and one output. In this paper, it is proposed to use a multi-input, multi-output approach. In particular, each algorithm will relate all the inputs to one output at a time (i.e. all inputs are mapped to internal pressures, then all the inputs are mapped again to the axial forces). Therefore, two distinctive equations are obtained as shown below.

The inputs used here are: $MinT_t$, $MaxT_t$: minimum and maximum thickness (mm) at the area of the non-circular protrusion at time t , MD_t : maximum vertical displacement (mm) within the area of the non-circular protrusion at time t , KE_t : average kinetic energy (mJ) of the whole deformed part at time t , IE_t : average internal energy (mJ) of the whole deformed part at time t , HS_t : maximum hoop stress (MPa) within the area of the non-circular protrusion at time t , AS_t : maximum axial stress (MPa) within the area of the non-circular protrusion at time t , MS_t : maximum principal strain within the area of the non-circular protrusion at time t . The outputs are: IP_t : internal pressure (MPa) at time t , AL_t : axial load (N/mm) at time t .

After training the machine learning algorithms discussed in the previous sections, algorithms are automatically assessing their results and calculate a score of accuracy (coefficient of determination) ("As of July 2020, scikit-learn.org, Linear Regression ") [23]. The best possible score of accuracy is 1.0 and can be defined as:

Score of accuracy = $(1 - \frac{u}{v})$, where

$$u = \sum (y_{true} - y_{predicted})^2$$


$$v = \sum (y_{true} - y_{true\ mean})^2$$

y_{true} = A True value of output,

$y_{predicted}$ = Predicted value of output.

The final arrangements of accuracy scores of the machine learning algorithms trained are given in Table 3.

Table 3: Arrange of Accuracy Scores of the Trained Machine Learning Algorithms

Machine learning algorithm	Arrange of accuracy scores
Multiple Random forest	<p>Higher</p> 
Multiple Decision tree	
Multiple Ridge regression	
Multiple Elastic net regression	
Multiple Linear regression	
Multiple Lasso regression	

Based on the results obtained, the most promising machine learning algorithms are the Random Forest and the Decision Tree. However, both Decision Tree and Random Forest cannot be reduced to explicit equations or inequalities. Hence, those methods cannot be incorporated into the AHNM model. The reason is that those models represent a tree structure (or collections of trees of data) that by nature do not lend themselves to equation or inequalities form. Therefore, the third-best candidate is Ridge Regression. Regression methods, in general, are representable in equations, and the coefficients obtained could give insights into how the outputs are affected by the inputs and vice versa. Applying the Multiple Ridge Regression as it is scoring the highest accuracy, the equations relating inputs and outputs of the FEA are:

$$IP_t = 1.794648 + 0.099449 MinT_t + 0.06269 MaxT_t - 0.04937 MD_t - 0.00056779 KE_t + 0.00030773 IE_t + 0.00381359AS_t + 0.00225969 HS_t + 0.18261735 MS_t \quad (1)$$

$$AL_t = 24.12692 + 8.260599 MinT_t + 2.18032 MaxT_t + 0.707943356 MD_t - 2.85718919 \times 10^{-3} KE_t + 4.85440054 \times 10^{-4} IE_t - 6.90207861 \times 10^{-2} AS_t + 7.48092522 \times 10^{-2} HS_t - 4.57685 MS_t \quad (2)$$

2.4. Adaptive heuristic nonlinear mathematical (AHNM) model

The objective of the proposed model is to obtain the optimum loading path, internal pressure and axial load, that are applied simultaneously to the tube, where the non-circular protrusion and the whole tube will follow to obtain the final shape. A Multi Linear Regression will learn the causal relations between the different parameters to be able to formulate mathematical forms that explain these relations, and then optimize these mathematical

forms, taking into consideration the wrinkling and thinning indicators.

Model's indicators

To account for the wrinkling, the literature proposed several indicators to be used to optimize the hydroforming process. In this paper, a closed-form wrinkling criteria based on instability of thin-walled tubes, Mellor [24] and Jain [25] is used to formulate the AHNM model as given in Eq. (3):

$$\epsilon_{critical} = \frac{2}{3}n \sqrt{\left(\frac{\sigma_{axial}}{\sigma_{hoop}}\right)^2 - \frac{\sigma_{axial}}{\sigma_{hoop}} + 1} \quad (3)$$

where $\epsilon_{critical}$ is the strain at which instability occurs, n is the hardening exponent, σ_{axial} is the axial stress within the tube, and σ_{hoop} is the circumferential stress within the tube.

It is assumed that the axial and the hoop stresses are approximately equal to the maximum and the second maximum principal stresses obtained from the FEA simulations. Eq. (3) will be incorporated into the model proposed below. Necking indicator used accounts for the minimum thickness of the model and must not be less than a minimum allowable thickness constraint (MIAT).

AHNM model development

The nonlinear mathematical model variables are:

Objective function Minimize.

$$\sum_{t=1}^N (IP_t + AL_t) \quad (4)$$

where t is the period (1 to N) and N is the total number of periods

Constraints:

$$IP_t = 1.794648 + 0.099449 MinT_t + 0.06269 MaxT_t - 0.04937 MD_t - 0.00056779 KE_t + 0.00030773 IE_t + 0.00381359AS_t + 0.00225969 HS_t + 0.18261735 MS_t \quad (5)$$

$$AL_t = 24.12692 + 8.260599 MinT_t + 2.18032 MaxT_t + 0.707943356 MD_t - 2.85718919 \times 10^{-3} KE_t + 4.85440054 \times 10^{-4} IE_t - 6.90207861 \times 10^{-2} AS_t + 7.48092522 \times 10^{-2} HS_t - 4.57685 MS_t \quad (6)$$

$$MS_t \leq \frac{2}{3}n \sqrt{\left(\frac{AS_t}{HS_t}\right)^2 - \frac{AS_t}{HS_t} + 1} \quad (7)$$

$$AS_t = HS_t + C, \text{ where } C \text{ is a constant} \quad (8)$$

$$MD_{t+1} = MD_t + S, \text{ where } S \text{ is a constant of maximum allowable vertical displacement per period} \quad (9)$$

$$KE_t \leq IE_t * Y, \text{ where } Y \text{ is a constant between } 5\text{-}10\% \quad (10)$$

$$MIAS \leq AS_t, HS_t \leq MAS, \text{ where } MIAS \text{ is the minimum allowable deformation stress, and the } MAS \text{ is the maximum allowable deformation stress} \quad (11)$$

$$MIAT \leq MinT_t \leq MAT, \text{ where } MIAT \text{ is minimum allowable thickness and } MAT \text{ is the maximum allowable thickness} \quad (12)$$

$$MD_N = FH, \text{ where } N \text{ is the last period, and } FH \text{ is the final height of the non-circular protrusion} \quad (13)$$

$MinT_t, MaxT_t, MD_t, KE_t, IE_t, AS_t, HS_t, MS_t \in R^+$, where R^+ is the set of positive real (14)

The objective function (4) is to minimize the total internal pressures and axial loads during the hydroforming process to reduce the system forming requirements and minimize the production costs. Constraints (5) and (6), using the ridge regression, represent the relations between the outcomes of the several FEAs of the hydroforming process of the non-circular protrusion. Constraint (7) ensures that the maximum strain in the deformed part including the non-circular protrusion does not exceed the strain that could cause plastic instability. Constraint (8) ensures that the axial and the hoop stresses induced in the deformed part are close to each other from the point of value. This condition is necessary to be able to use the wrinkling criterion in Constraint (7). Constraint (9) ensures that the maximum height of the non-circular protrusion is within a specific limit at each step. Constraint (10) keeps the ratio between the average kinetic and internal energy of the deformed body constant. Constraint (11) puts upper and lower limits of the axial and hoop stresses to enable the hydroforming process without excessive stresses. Constraint (12) ensures that the minimum thickness of the protruded section does not exceed or fall under specific limits. This constraint is dedicated to avoiding thinning phenomena. Constraint (13) limits the maximum height that could be achieved by the non-circular protrusion to a specific value. Constraint (14) guarantees that the values of all variables are real positive numbers.

3. Results and discussion of proposed AHNM model

The AHNM model is implemented using Pyomo, an open-source optimization formulation models written in Python language with a diverse set of optimization capabilities. Since Pyomo is not a solver but a mathematical algebraic modelling language, a solver named IPOPT (Interior Point OPTimizer) is used to solve the nonlinear AHNM model. To solve the model, the following parameters are used:

$N = 10$ periods, $C = 5$ MPa, $S = 2$ mm, $Y = 5\%$, $MIAS = 300$ MPa, $MAS = 340$ MPa, $MIAT = 0.15$ mm, $MAT = 0.3$ mm

The output value of the objective function was 42.5, which represents the average of the total algebraic summation of internal pressures and axial loads that are used through the total hydroforming period. The model can obtain a minimum thickness of 0.15 mm in the non-circular protrusion part. The optimized maximum axial stress in the deformed part is 300 MPa, and the optimized maximum hoop stress is 295 MPa. The maximum principal strain to avoid plastic instability (wrinkling and necking) is 0.363. It should be noted that the maximum allowed vertical displacement per period is 2 mm. The optimum results for the internal and axial load obtained are shown in Figure 6.

The results of the optimized AHNM model provide useful insight into how to balance the progress of both the internal pressure and the axial load. The AHNM model optimizes the loading path to a linear path as shown in Figure 6, since it is calculated through a balance between both the internal and the axial load. The axial load at the beginning of the forming process

begins at the lowest value (approx. 30 N/mm), then it slowly increases to reach 43 N/mm. Concurrently, the internal pressure began at the highest value at 6.3 MPa, and slowly decreases to 5.4 MPa. This gradual axial load increase supports the deformed non-circular protrusion in addition to the rest of the deformed tube. The model balances the different aspects of the hydroforming process, where restrictions on stresses, minimum thicknesses, and maximum vertical displacement are taken into consideration. Due to Constraint (7), the model also decreases the occurrence of plastic instability that ranges from wrinkling to necking. It is noteworthy that the obtained pressures and axial loads are not from those values in which the Ridge Regression and the other machine learning algorithms were trained on. However, the AHNM is able to predict these pressures and forces from the relations that are obtained from the ML algorithms.

The previously obtained paths of internal pressure and axial load show that the optimum path is always linear with equal steps of protrusion height. The effect of the loading steps on the system requirements (summation of internal pressure and axial load at certain protrusion height) and the maximum protrusion height can be reached for the tee joint is also investigated. The maximum displacement at each step and the number of steps are varied using a random number generator script written in Python to generate different arrays of steps while keeping the sum of steps to 20 mm. In the previous study, there were 10 equal steps, where each step would increase the height of the protrusion by 2 mm. Table 4 shows different arrays of steps which are solved using the AHNM model to produce new forming paths. For example, in Array No. 2, the first step will increase the protrusion height by 2mm, then 2 mm, then 1 mm, etc.

Each array steps express the input in the AHNM model, where the output is an internal pressure value and axial load value at each step (loading path). Comparing these values indicates that the step numbers and values of each array are affecting directly the solver objective function. The minimum values for the objective function are for Arrays No. 5 and No. 7 with values of 40.7 and 39.71, respectively. The differences between the results of the internal pressure and axial load of each array cause the difference in the objective function, while the boundaries (first and last) values are almost the same. This shows the consideration of physical process parameter by the AHNM model. Noteworthy that, the internal pressure and axial load versus the protrusion height for all arrays is straight lines with identical slope.

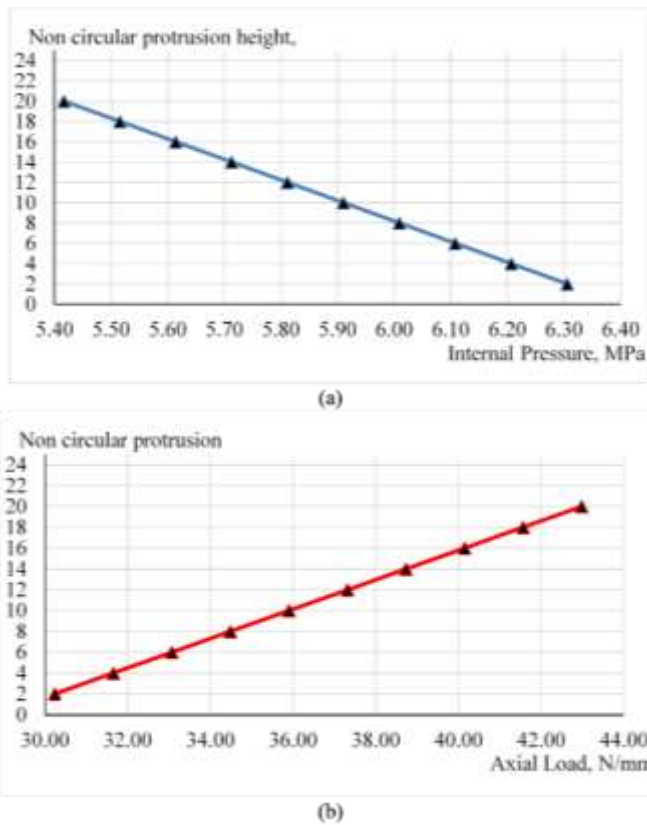


Figure 6: Optimized AHNM Progress of (a) Internal Pressure and (b) Axial Load Through Non-Circular Tube Hydroforming

Table 4: The Arrays of Various Steps On the Vertical Displacement

Array No.	No.1	No. 2	No. 3	No. 4	No.5	No.6	No.7
No. of steps	10	10	10	10	10	50	50
Steps values	2,2 ,2,2 ,2,2 ,2,2 ,2,2	2,2 ,1,1 ,5,2 ,3,2 ,1,1	2,3 ,2,1 ,2,1 ,5,1 ,2,1	1,3 ,2,1 ,1,1 ,5,2 ,1,3	0.004, 0.508, 1.267, 1.719, 2.106, 2.468, 2.848, 3.254, 3.678, 2.148	0.001, 0.408143 *(49)	0.001 ,0.0173 (0.001 +0.1628) ,0.0336 (0.0173 +0.1628)etc.
O.F Value	$\sum_{i=1}^N (IP_t + AL_t) / (\text{No. of steps})$						
	42.5	42.7	42.8	41.9	40.7	41.8	39.71

4. Conclusions and future work

Although the AHNM model is linear, the results obtained showed the ability of the ML algorithms to be improved to optimally predict and understand the incremental internal pressure and the axial load needed to accomplish the hydroforming process. The solution time is in milliseconds, and nearly instantaneous, which allowed the testing, development,

and examining of different variables affecting the hydroforming process of an elliptical protrusion. A sensitivity analysis was performed regarding the effect of mesh size. The values of steps of the non-circular protrusion height, and the number of steps, are directly affect the optimum loading path needed to successively complete the hydroforming process.

Since the optimization model proposed contained nonlinear constraint and was solved using interior-point optimizer, then the solution is not guaranteed to be the global optimum. As the process is highly non-linear, an additional effort is required either to linearize the nonlinear constraint or to produce sufficient mathematical conditions to ensure more compatibility with the high non-linearity of the process and be closer to the global optimality

Other parameters that could affect the tube hydroforming process (such as coefficient of friction, applying the internal pressure at different times than the axial loads can be applied – the axial load my delayed in application after applying internal pressure – and counter punch force) can be added examined and incorporated to the AHNM model.

Conflict of Interest

The authors declare no conflict of interest.

Acknowledgment

This research was partially supported by Misr Elgawda Company for Manufacturing & Trading, and Mechanical Design & Production department of Faculty of Engineering, Cairo University. I am thankful to my esteemed and professional colleagues in these two entities, who provided expertise that greatly assisted the research, and for their comments on an earlier version of the manuscript, that improved the manuscript significantly.

References

- [1] J. E. Gray, A. P. Devereaux, and W. M. Parker, "Apparatus for making wrought metal T's," Google Patents, 1940.
- [2] M. Ahmetoglu, and T. Altan, "Tube hydroforming: state-of-the-art and future trends," Journal of Materials Processing Technology, vol. 98, no. 1, pp. 25-33, 2000.
- [3] M. Ahmetoglu, K. Sutter, X. Li et al., "Tube hydroforming: current research, applications and need for training," Journal of materials processing technology, vol. 98, no. 2, pp. 224-231, 2000.
- [4] A. Alaswad, K. Benyounis, and A. Olabi, "Tube hydroforming process: A reference guide," Materials & Design, vol. 33, pp. 328-339, 2012.
- [5] P. V. Reddy, and B. V. Reddy, "Effect of Tube Material and Heat Treatment Temperatures on Tube Formability During Tube Hydroforming Process," Journal of The Institution of Engineers (India): Series C, vol. 101, no. 6, pp. 991-998, 2020.
- [6] K.-J. Fann, and P.-Y. Hsiao, "Optimization of loading conditions for tube hydroforming," Journal of Materials Processing Technology, vol. 140, no. 1-3, pp. 520-524, 2003.
- [7] S.-W. Kim, W.-J. Song, B.-S. Kang et al., "Bursting failure prediction in tube hydroforming using FLSD," The International Journal of Advanced Manufacturing Technology, vol. 41, no. 3-4, pp. 311-322, 2009.
- [8] R. Di Lorenzo, G. Ingarao, and F. Chinesta, "Integration of gradient based and response surface methods to develop a cascade optimisation strategy for

Y-shaped tube hydroforming process design,” *Advances in Engineering Software*, vol. 41, no. 2, pp. 336-348, 2010.

- [9] M. Mirzaali, G. Liaghat, H. M. Naeini et al., “Optimization of tube hydroforming process using simulated annealing algorithm,” *Procedia Engineering*, vol. 10, pp. 3012-3019, 2011.
- [10] F. Abbassi, F. Ahmad, S. Gulzar et al., “Design of T-shaped tube hydroforming using finite element and artificial neural network modeling,” *Journal of Mechanical Science and Technology*, pp. 1-10, 2020.
- [11] A. Fiorentino, P. S. Ginestra, A. Attanasio et al., “Numerical Optimization of the Blank Dimensions in Tube Hydroforming Using Line-Search and Bisection Methods,” *Materials*, vol. 13, no. 4, pp. 945, 2020.
- [12] A. Aydemir, J. De Vree, W. Brekelmans et al., “An adaptive simulation approach designed for tube hydroforming processes,” *Journal of materials processing technology*, vol. 159, no. 3, pp. 303-310, 2005.
- [13] S. Heo, J. Kim, and B. Kang, “Investigation on determination of loading path to enhance formability in tube hydroforming process using APDL,” *Journal of materials processing technology*, vol. 177, no. 1-3, pp. 653-657, 2006.
- [14] K.-i. Manabe, M. Suetake, H. Koyama et al., “Hydroforming process optimization of aluminum alloy tube using intelligent control technique,” *International Journal of Machine tools and manufacture*, vol. 46, no. 11, pp. 1207-1211, 2006.
- [15] S.-h. Li, B. Yang, W.-g. Zhang et al., “Loading path prediction for tube hydroforming process using a fuzzy control strategy,” *Materials & Design*, vol. 29, no. 6, pp. 1110-1116, 2008.
- [16] K.-i. Manabe, X. Chen, D. Kobayashi et al., “Development of in-process fuzzy control system for T-shape tube hydroforming,” *Procedia Engineering*, vol. 81, pp. 2518-2523, 2014.
- [17] N. Abedrabbo, M. Worswick, R. Mayer et al., “Optimization methods for the tube hydroforming process applied to advanced high-strength steels with experimental verification,” *Journal of Materials Processing Technology*, vol. 209, no. 1, pp. 110-123, 2009.
- [18] A. Abdelkefi, P. Malécot, N. Boudeau et al., “On the tube hydroforming process using rectangular, trapezoidal, and trapezoid-sectional dies: modeling and experiments,” *The International Journal of Advanced Manufacturing Technology*, vol. 93, no. 5-8, pp. 1725-1735, 2017.
- [19] A. B. Miguel, “Machine Learning In Mechanics: Simple Resources, Examples & Opportunities,” *Journal Club*, 2020.
- [20] scikit-learn.org. "https://scikit-learn.org/stable/tutorial/machine_learning_map/index.html."
- [21] F. Andreis, “Shrinkage methods and variable selection: Ridge, Lasso, and Elastic Nets,” 2017.
- [22] T. Prajwala, “A comparative study on decision tree and random forest using R tool,” *International journal of advanced research in computer and communication engineering*, vol. 4, no. 1, pp. 196-199, 2015.
- [23] scikit-learn.org. "https://scikit-learn.org/stable/modules/generated/sklearn.linear_model.LinearRegression.html."
- [24] P. Mellor, “Tensile instability in thin-walled tubes,” *Journal of Mechanical Engineering Science*, vol. 4, no. 3, pp. 251-256, 1962.
- [25] N. Jain, “Modeling and analysis of dual hydroforming process,” *Texas A&M University*, 2004.

Appendix (A)

Sr.	Internal pressure	Axial force	min thickness	max thickness	Protrusion height	avg_kinetic_energy	Avg.intern al_energy	max. axial stress	max. hoop stress	Max. strain
	Mpa	N/mm	mm	mm	mm	m.Joule	m.Joule	Mpa	Mpa	
1	3	26	0.2000	0.2001	0.0186	0.0114	57.0556	191.4234	191.3049	0.0001
2	3	27	0.2000	0.2001	0.0188	0.0115	58.4184	193.9088	193.8744	0.0002
3	3	28	0.2000	0.2001	0.0190	0.0117	59.8181	198.0152	197.8375	0.0003
4	3	29	0.2000	0.2001	0.0192	0.0118	61.2596	206.1028	205.8819	0.0004
5	3	30	0.2000	0.2001	0.0199	0.0120	62.7644	223.7656	223.4652	0.0007
6	3	31	0.2000	0.2001	0.0277	0.0122	64.4460	218.9582	218.5411	0.0018
7	3	32	0.1999	0.2005	0.2443	0.0940	74.2745	292.6276	280.7490	0.0291
8	3	33	0.1993	0.2006	0.6047	0.6270	114.6001	318.5265	298.9641	0.0483
9	3	34	0.1953	0.2121	1.4754	2.0785	198.0988	319.0298	318.8756	0.1767
10	4	26	0.1949	0.2009	1.4942	3.0630	670.1483	318.5616	317.6994	0.1129
11	4	27	0.1938	0.2067	1.8512	4.6903	785.6933	318.6682	318.5539	0.1473
12	4	28	0.1925	0.2169	2.2735	7.2686	911.9425	319.1902	318.6080	0.2521
13	4	29	0.1867	0.2425	3.1208	18.6244	1096.4772	320.2469	320.8145	0.6783
14	4	30	0.1808	0.2429	4.0760	78.0195	1371.9486	344.8228	339.4066	0.5910
15	4	31	0.1801	0.3892	4.9025	186.0417	1796.8985	325.6680	357.6669	1.9908
16	5	26	0.1884	0.2113	4.3821	49.3106	3287.5227	319.0443	318.8345	0.3723
17	5	27	0.1884	0.2151	4.6350	57.0155	3460.5523	319.1562	317.3199	0.3963
18	5	28	0.1883	0.2152	4.9199	66.5774	3635.5680	318.1945	319.0578	0.4138
19	5	29	0.1879	0.2179	5.1486	77.2440	3818.0128	318.3931	319.3716	0.4405
20	5	30	0.1878	0.2232	5.5316	88.8924	4005.3164	319.5698	318.3752	0.4620
21	5	31	0.1876	0.2290	6.0509	102.6367	4206.5666	319.0847	318.6105	0.4923
22	5	32	0.1876	0.2365	6.6720	118.9098	4419.5772	319.4340	319.2233	0.5250
23	5	33	0.1881	0.2425	7.3345	137.8943	4646.7379	318.8747	319.9839	0.5801
24	5	34	0.1886	0.2479	7.9961	160.6842	4888.5950	318.9688	319.2912	0.6653
25	5	35	0.1892	0.2521	8.7054	186.4522	5139.3093	318.9074	318.7920	0.7418
26	5	36	0.1900	0.2572	9.4868	215.9533	5406.7169	318.5141	319.1826	0.8291
27	5	37	0.1907	0.2595	10.2083	249.2859	5687.0561	318.8894	357.1854	0.8633
28	5	38	0.1915	0.2604	10.7955	284.7461	5968.6107	314.8751	353.2955	0.8712
29	5	39	0.1920	0.2605	11.4035	324.2320	6263.9818	316.3286	354.3741	0.8742
30	5	40	0.1910	0.2604	12.1333	366.7869	6570.9068	318.6487	353.3761	0.8755

31	6	26	0.1634	0.2281	12.6121	374.5482	7937.5469	319.5815	319.3662	0.7683
32	6	27	0.1642	0.2329	13.1376	409.3883	8169.3554	319.4843	319.6591	0.7853
33	6	28	0.1649	0.2319	13.7077	445.7426	8409.0888	317.1463	319.0305	0.7994
34	6	29	0.1653	0.2371	14.2606	484.5914	8652.9718	318.2832	318.6976	0.8138
35	6	30	0.1659	0.2382	14.8400	526.4630	8904.3050	317.1594	318.6645	0.8292
36	6	31	0.1664	0.2407	15.4175	570.1203	9161.9421	317.4857	317.9878	0.8460
37	6	32	0.1671	0.2437	15.9932	615.1258	9425.1353	315.4202	319.6006	0.8624
38	6	33	0.1682	0.2449	16.5852	663.4803	9696.6318	318.5674	319.7949	0.8804
39	6	34	0.1688	0.2477	17.1762	714.7423	9978.4684	318.4283	318.2563	0.8980
40	6	35	0.1696	0.2498	17.7544	765.1055	10258.939	318.6850	318.5635	0.9159
41	6	36	0.1702	0.2515	18.3660	822.6155	10560.995	319.2977	318.7357	0.9347
42	6	37	0.1715	0.2538	18.9975	884.9566	10879.960	318.8527	319.7320	0.9545
43	6	38	0.1723	0.2567	19.6113	945.8481	11196.489	318.4601	320.4799	0.9753
44	6	39	0.1730	0.2611	20.2021	1001.8185	11497.378	319.7740	321.0491	0.9943
45	6	40	0.1742	0.2625	20.8869	1075.6273	11858.414	318.3438	319.1384	1.0177
46	7	29	0.0051	0.2300	25.4460	1706.9802	14136.260	354.4324	341.3822	2.3196
47	7	30	0.0091	0.2333	25.9262	1734.6505	14424.859	356.5959	357.0408	2.1150
48	7	31	0.0157	0.2362	26.6264	1789.5863	14710.857	354.6410	337.7912	1.9143
49	7	32	0.0491	0.2392	26.9122	1855.2540	15002.815	357.9521	352.6538	1.2625
50	7	33	0.1094	0.2422	27.4204	1929.3315	15320.064	319.7207	321.3746	1.1660
51	7	34	0.1315	0.2449	28.0235	2008.9141	15656.094	318.3130	332.2327	1.2145
52	7	35	0.1456	0.2474	28.6695	2092.2536	16007.172	318.3230	322.9135	1.2541
53	7	36	0.1506	0.2500	29.3743	2179.5852	16371.363	317.8943	321.3615	1.2959
54	7	37	0.1522	0.2569	30.0029	2270.3201	16744.128	318.7203	320.9495	1.3356
55	7	38	0.1536	0.2620	30.6270	2364.7165	17123.574	318.1297	322.0998	1.3740
56	7	39	0.1551	0.2615	31.2606	2462.8171	17512.535	318.4039	322.0403	1.4085
57	7	40	0.1561	0.2611	31.9079	2564.5174	17910.458	321.3089	319.7015	1.4557